THE ASTROPHYSICAL JOURNAL, 450:111–121, 1995 September 1


# NEAR-INFRARED IMAGING AND SPECTROSCOPY OF THE BRIGHT *IRAS* GALAXY VV 114

RENÉ DOYON,[1] DANIEL NADEAU,[1] R. D. JOSEPH,[2] J. D. GOLDADER,[2] D. B. SANDERS,[2] AND NEIL ROWLANDS[1]

*Received 1993 November 10; accepted 1995 March 13*

## ABSTRACT

We present sub-arcsecond (FWHM $<0\farcs7$) *R*, *J*, *H*, *K*, and *L'* images of the bright *IRAS* galaxy VV 114 obtained on the Canada-France-Hawaii Telescope and the NASA Infrared Telescope Facility. These observations have unveiled two very strong infrared (IR) sources (VV 114 East) located $\sim 15''$ east of the main optical nucleus (VV 114 West). These two sources, separated by $1\farcs6$ and spatially resolved at 2.2 $\mu$m, are much brighter in the infrared than the optical peak is. We have also secured medium resolution ($\lambda/\Delta\lambda = 330$) *K*-window spectra of both regions of VV 114 using the long-slit, cooled grating spectrometer CGS4 on the United Kingdom Infrared Telescope. While the strongest activity is found in VV 114 East, both VV 114 West and VV 114 East show strong recombination lines of hydrogen and helium, several transitions of molecular hydrogen, and relatively deep CO bands at 2.3 $\mu$m. These spectral features are signatures of vigorous star formation activity. The $H_2$ spectra show evidence of UV fluorescence excitation. From the spatial extent of Br$\gamma$ in VV 114 East, we infer that this region has a population of $4 \times 10^5$ O8V stars. Such a cluster of early-type stars can account for more than half the *IRAS* luminosity.

We fit the spectral energy distributions (SEDs) of the newly discovered IR sources with a simple three-component model. Based on observed *RJHKL'* colors and the strength of the 2.3 $\mu$m CO band, this model can determine the absolute extinction at 2.2 $\mu$m and the fraction of the *K* continuum contributed by hot dust and nebular emission. We find that both IR sources in VV 114 East suffer from an extinction $A_K$ of $\sim 0.4$ mag. In the strongest of the two IR sources, emission from hot dust contributes more than 55% of the *K* continuum, nebular emission contributes 5%, and late-type red supergiant stars make up the remainder. The *JHK* colors of VV 114 West strongly suggest that a large fraction of the structure seen in this region is due to the presence of numerous H II regions.

We make crude measurements of the rotation curves of the systems using several emission lines. The velocity gradient observed in VV 114 East implies a mass enclosed within $r < 1.1$ kpc of $9 \times 10^9\ M_\odot$, which is similar to the mass distribution of our Galaxy within the same radius. A similar velocity gradient is inferred for VV 114 West.

Our infrared images and spectroscopic observations provide a self-consistent picture of VV 114 as an interacting system involving a merger and another galaxy of approximately equal mass, in which vigorous starburst activity is taking place. There is no evidence for active galactic nuclei in VV 114.

*Subject headings:* galaxies: individual (VV 114) — galaxies: interactions — galaxies: photometry — infrared: galaxies

## 1. INTRODUCTION

One important result of the *IRAS* survey is the discovery of a class of galaxies with far-infrared (FIR) luminosities in excess of $10^{11}\ L_\odot$, referred to as the *IRAS* Bright Galaxy Sample (Soifer et al. 1987; Soifer et al. 1989). It is generally accepted that this infrared (IR) excess is associated with vigorous star formation (starburst) activity (e.g., Joseph, Wright, & Wade 1984; Joseph & Wright 1985; Rieke et al. 1980) and/or buried active galactic nuclei (AGNs) (e.g., Becklin & Wynn-Williams 1987; Sanders et al. 1988). Since the most luminous of these galaxies (e.g., ARP 220) may represent a phase in the formation of quasars (Sanders et al. 1988), and because of the possible evolutionary link existing between starbursts and AGNs (Norman & Scoville 1988; Scoville & Norman 1988), understanding the nature of the FIR luminosities of bright *IRAS* galaxies is of prime importance.

Near-IR imaging and spectroscopy are excellent tools for studying the infrared emission of these galaxies. Since the extinction at 2.2 $\mu$m is only 1/10 of that in the optical, *K*-band imaging offers a better look at the true mass distribution, which helps in identifying the main centers of activity. Near-IR colors are also very useful for estimating the extinction and the relative contributions of nebular and hot-dust emission to the 2.2 $\mu$m continuum (e.g., Telesco, Decher, & Gatley 1985). The detection of extended IR emission provides a simple and yet powerful argument for excluding the presence of an AGN in a galaxy.

The *K*-band window offers several diagnostic spectral lines for studying the young stellar populations of starbursts. Narrow emission lines of He I 2.06 $\mu$m and Br$\gamma$ provide some constraints on the relative number of OB stars (Doyon, Puxley, & Joseph 1992). The deep CO band absorption longward of 2.3 $\mu$m arises from the atmosphere of late-type stars, and its luminosity dependence makes it a very good tool for estimating the ratio of giants to supergiants. This window is also the site of many transitions of molecular hydrogen ($H_2$), and such an emission is conspicuous in starbursts and AGNs. In general, starbursts tend to show relatively strong emission

[1] Département de Physique, Université de Montréal and Observatoire du Mont Mégantic, C. P. 6128, Succursale Centre Ville, Montréal, QC, Canada, H3C 3J7.

[2] Institute for Astronomy, University of Hawaii, 2680 Woodlawn Drive, Honolulu, HI 96822.

lines with underlying stellar continua showing absorption lines, the strongest being the CO band. On the contrary, emission lines of AGNs have small equivalent widths, and their underlying continua are very red, with relatively weak absorption lines (e.g., NGC 1068; Thompson, Lebofsky, & Rieke 1978). IR spectroscopy also offers the advantage that buried broad-line regions characteristic of AGNs can be detected with Br$\gamma$.

In this paper, we present sub-arcsecond *RJHKL'* images and medium resolution *K*-band spectra of the bright *IRAS* galaxy VV 114. These observations were obtained as part of a broader and long-term program to determine the near-IR photometric and spectroscopic properties of bright *IRAS* galaxies. *K*-band spectroscopy of the ultraluminous ($L_{IR} \geq 10^{12}\ L_{\odot}$) sample is described in Goldader et al. (1995).

VV 114 (IC 1623, ARP 236) is distinguished by its very peculiar optical image, which shows several hot spots (Scoville et al. 1989). At a distance of 77 Mpc ($H_0 = 75$ km s$^{-1}$ Mpc$^{-1}$), it has a total luminosity (8–1000 $\mu$m) of $4.2 \times 10^{11}\ L_{\odot}$ (Sanders, Scoville, & Soifer 1991). Like many luminous *IRAS* galaxies, VV 114 is very rich in molecular gas (Yun, Scoville, & Knop 1994). Sanders et al. (1991) described this object as a merging pair. Based on optical spectra, both Allen et al. (1991) and Sanders et al. (1991) concluded that this galaxy is a starburst, an hypothesis which is also supported by the *IRAS* colors (Condon et al. 1991). The data presented in this paper concur with their conclusion and add further evidence that this object is a starburst. We also report the detection of two bright IR sources which are barely detected in the visible. The optical/infrared morphology of VV 114 is also described in Knop et al. (1994).

## 2. OBSERVATIONS AND DATA REDUCTION

### 2.1. *Imaging*

Near-IR images of VV 114 at *J* (1.25 $\mu$m), *H* (1.65 $\mu$m), and *K* (2.2 $\mu$m) were obtained on the Canada-France-Hawaii Telescope (CFHT) during two observing runs: 1991 September 21 and 1992 November 10. The images were obtained with MONICA (Montreal Infrared Camera). This instrument is equipped with a 256 × 256 HgCdTe NICMOS3 detector manufactured by Rockwell International. The camera features *JHK* filters, polarizers, a circular variable filter which provides a 1.4% narrow-band imaging capability from 1.5 to 2.5 $\mu$m and a polarimetry mode. The details of this instrument are described in Nadeau et al. (1994). At the f/8 Casse grain focus of the CFHT, the cold reimaging optics of MONICA yield a plate scale of 0".25 pixel$^{-1}$.

The seeing conditions were excellent during both runs, averaging 0".5 and 0".7 in 1991 September and 1992 November, respectively. A typical set of observations consisted of an integration of 2–5 minutes on the galaxy followed immediately by a sky frame with the same integration time. After subtracting a dark frame, all images were flat-fielded with a sky flat defined by the median of several sky frames. Since the galaxy covered a relatively small area of the detector, sky subtraction was achieved by subtracting each frame by its mode. The images were then corrected for bad pixels, corrected for geometrical distortion, registered, and co-added. The same operation was repeated for each band.

The total integration time of the final images is 900, 240, and 840 s at *J*, *H*, and *K*, respectively. The images were flux calibrated using UKIRT Faint Standard Stars (Casali & Hawarden 1992). Based on the photometry of several standard stars taken on two different runs, we estimate a photometric uncertainty (excluding the uncertainty on the absolute magnitude scale) of ~6%. Our photometry is, within the uncertainties, consistent with the aperture photometry of Carico et al. (1988).

An image of VV 114 at *R* (0.65 $\mu$m) was also obtained at the prime focus of the CFHT on 1993 June 10. The instrument used was FOCAM, a CCD camera built around an 1024 × 680 RCA chip. The image was obtained after an integration time of 300 s and reduced in a similar fashion as the near-IR images. The seeing for these observations was 0".8. Calibration was achieved with CFHT standard stars. The uncertainty of the photometric calibration at *R* is ~3%.

Complementary images of VV 114 were also taken at *H*, *K*, and *L'* (3.8 $\mu$m) on the NASA Infrared Telescope Facility (IRTF) using PROTOCAM, the facility IR camera of this observatory, on 1991 October 6. Three individual images were obtained, for a total integration time of 400 s. The flux calibration was achieved with observations of the star BS 718 (*L'* = 4.41). The photometric uncertainty at *L'* is ~0.2 mag. The relative *H* and *K* photometry between the PROTOCAM and MONICA observations are consistent within the uncertainties.

### 2.2. *Spectroscopy*

*K*-band spectra of VV 114 were obtained on the United Kingdom Infrared Telescope on the nights of 1991 September 19 and 22, using the long-slit cooled grating spectrometer CGS4, which is built around a 58 × 62 SBRC InSb array. More details about this instrument are given in Mountain et al. (1990). CGS4 was used with the 75 l mm$^{-1}$ grating in first order, providing a resolving power ($\lambda/\delta\lambda$) of 337 in the *K* band and a spectral coverage encompassing most of the *K* band. The plate scale was 3" per pixel, and the slit width was 1 pixel. The slit length was 30 pixels.

#### 2.2.1. *Observing Procedure*

Two slit positions were observed (see Fig. 2). The first spectrum was obtained on 1991 September 21 with the slit centered on the brightest optical peak as seen on the offset guider television. The original plan was to align the slit along the two brightest optical knots at a position angle of 115°. Unfortunately, the position angle was mistakenly set to a position angle of 105°. The second position, obtained on the night of 1991 September 22, was centered on the brightest *K* peak, discovered on the previous night with MONICA on CFHT. The position of this IR peak was measured from the *K* image to be 14" east and 3" south of the brightest optical knot. The slit was set at a position angle of 45° along the two brightest *K* peaks.

A typical observing sequence consists of the following. A single spectrum obtained with CGS4 is not fully sampled. Full sampling is achieved by fixing the grating and moving the array by half a pixel over two pixels, resulting in four wavelength-shifted images. Merging/co-adding these four image spectra together yields a fully sampled "combined" spectrum. This procedure also ensured that bad pixels were unambiguously removed in the combined spectrum. An integration time of 20 s was used for every spectrum, so the combined spectrum was effectively integrated for 80 s. The telescope was then moved to the sky 60" south of the galaxy, where two combined spectra (two sequences of four shifted spectra) were observed. The cycle was completed by taking a combined spectrum back on the galaxy. This cycle, object-sky-

sky-object, was repeated several times until the on-line data reduction software showed that we had reached an adequate signal-to-noise. The total integration times (excluding the sky) for the two spectra observed on the optical and infrared peaks were 1520 and 1440 s, respectively.

#### 2.2.2. *Data Reduction Procedure*

The following procedure was used to reduce the spectra. Most of the operations described below were achieved semi-automatically under the IRAF environment using IRAF scripts written by one of us (R. D.).

1. Before merging the four shifted spectra together to form a fully sampled combined spectrum, all four spectra are first subtracted by the corresponding adjacent sky frame. This operation eliminates the dark current, and, to a first order, the strong OH line emission from the sky.
2. All four spectra are then flat-fielded with a flat obtained by illuminating the array with a blackbody source available in the CGS4 calibration unit.
3. Any OH line emission residuals are eliminated by fitting a low-order polynomial (in general, a straight line) to the sky defined by the pixels at both ends of the slit. The "sky" pixels are chosen conservatively so as to avoid the signal from the galaxy.
4. At this point, the resulting four sky-subtracted images are merged together to form a combined image spectrum. Any spectrum extracted from this image is fully sampled by a factor of 2. However, if the signal from the object is relatively strong—which is always the case of stars, for instance—the four sky-subtracted images are not merged immediately. Instead, the four images are scaled such that all spectra extracted from the individual four sky-subtracted images have the same average signal. This operation is necessary, because in the process of taking the four shifted images, the signal may vary significantly due to wind bouncing and seeing variation, resulting in strong ripples in the combined spectrum if no scaling is applied. In this particular case, the signal from VV 114 was strong enough to apply a scaling factor.
5. All combined images are then co-added together. Again, a scaling factor is applied before the co-addition. This operation produces a co-added image spectrum and also an error image, which is used later for estimating error bars.
6. The co-added image is wavelength-calibrated using an argon lamp spectrum.
7. Because the CGS4 spectra were slightly misaligned (by 0.″4) with respect to the dispersion direction of the array (i.e., the spectra were slightly tilted), a geometric transformation was applied to the images to correct for this effect.
8. The atmospheric and instrument responses are corrected by dividing each row of the image obtained in (6) with the spectrum of a spectroscopic standard star. The result is then multiplied by a blackbody spectrum defined by the effective temperature and the absolute flux of the standard star. The same operation is applied to the error image. At this point, flux-calibrated spectra (with error bars) can be extracted from this image.

SAO 147622 (F2 V; $T_{\rm eff} = 7200$ K) was used as spectroscopic standard for correcting the spectra of VV 114. Based on observations of several flux standards taken on different nights, we estimate a $K$ magnitude of 4.6 for this star. We estimate that the spectrophotometric accuracy of our spectra is $\sim 15\%$.

## 3. RESULTS

### 3.1. *Imaging*

Contours of optical ($R$) and infrared ($JHKL'$) emission are shown in Figure 1. Like the optical images, the IR images show a wealth of structure. The brightest optical knots seen on the galaxy all have infrared counterparts. However, the morphology differs drastically $\sim 15''$ east of the main optical peak where the IR images show two very strong sources separated by 1.″6. Those sources are barely detected in the $R$ image, and yet, in the infrared, the brightest of the two sources at $K$ is 5 times brighter (within a circular aperture of 1″) than the source coincident with the brightest optical peak. The optical and near-IR images qualitatively suggest that the two eastern IR sources suffer from relatively high extinction. As shown in Figure 1, the relative brightness of the new IR sources varies considerably as a function of wavelength. It is also clear from Figure 1 that the easternmost feature seen in the $R$ band appears in the infrared as a faint tidal tail. The two bright sources seen in the $JHK$ images are clearly detected at $L'$. Taking into account the higher spatial resolution of our observations, our images are morphologically very similar to those obtained by Knop et al. (1994). Hereafter, we shall refer to both regions of VV 114 as VV 114E (east) and VV 114W (west).

We have noted four sources of interest from the $K$ image. Those are annotated in the $K$-band image of Figure 2 by the letters A, B, C, and D, in decreasing order of their $K$ flux defined within a circular aperture of 1″. In this notation, the brightest optical peak corresponds to source C. Optical/infrared aperture photometry and relative positions of these sources are given in Table 1.

Source A is not only the brightest IR source, it is also the reddest. With an $H-K$ of 1.42, this source is at least as red as IR 0857+3915, which is the reddest of the ultraluminous infrared galaxies observed by Sanders et al. (1988). There is no optical counterpart for source A, but source B is displaced by only 0.″5 from an optical knot seen in the $R$ image (see Fig. 1). Given the uncertainties in the relative orientations and plate scales of the $R$ and near-IR images, we cannot exclude the possibility that source B is coincident with this optical knot. Because of this uncertainty, the $R$-magnitude of source B given in Table 1, measured 0.″5 away from the optical knot, could be systematically underestimated by $\sim 20\%$. Knop et al. (1994) showed that sources A and B are within the uncertainties coincident with the double radio source detected by Condon et al. (1991). The position derived from the radio data for source A is $\alpha_{1950} = 01^{\rm h}05^{\rm m}19^{\rm s}.82$, $\delta_{1950} = -17°46'25''.7$.

A faint star was detected on the $JHK$ images of VV 114, allowing an accurate characterization of the point spread function (PSF). Comparing this PSF with cuts through sources A, B, C, and D on the $K$ image clearly shows that all sources are extended at 2.2 $\mu$m. The most compact source is A, with a deconvolved FHWM of 1.″04, corresponding to a linear distance of 390 pc. However, source A is not spatially resolved at $L'$ with a FHWM of 0.″3, which corresponds to the diffraction limit of the IRTF at 3.8 $\mu$m.

### 3.2. *Spectroscopy*

The two positions and orientations of the CGS4 slit are shown in Figure 2. Emission lines were detected on five positions along the slits for both VV 114W and VV 114E; those

TABLE 1

OPTICAL AND INFRARED PHOTOMETRY OF VV 114

| Position | $\Delta\alpha$ | $\Delta\delta$ | Aperture[a] | $m_k$[b] | $R-K$ (mag) | $J-K$ (mag) | $H-K$ (mag) | $K-L'$ (mag) |
|---|---|---|---|---|---|---|---|---|
| A ..... | 0″ | 0″ | 1″ | 13.42 | 6.50 | 2.55 | 1.42 | 2.90 |
| | 0 | 0 | 2 | 12.36 | 6.10 | 2.22 | 1.18 | 2.44 |
| B ..... | 1.33 | 0.92 | 1 | 13.86 | 5.18 | 1.66 | 0.76 | 1.61 |
| | 1.33 | 0.92 | 2 | 12.67 | 5.00 | 1.61 | 0.70 | 1.52 |
| C ..... | −13.48 | 2.98 | 1 | 15.00 | 2.20 | 0.87 | 0.34 | ... |
| | −13.48 | 2.98 | 2 | 13.72 | 2.22 | 0.86 | 0.32 | ... |
| | −13.48 | 2.98 | 10 | 11.55 | 2.20 | 0.82 | 0.29 | ... |
| D ..... | −11.07 | −2.21 | 1 | 15.81 | 1.76 | 0.98 | 0.52 | ... |
| | −11.07 | −2.21 | 2 | 14.55 | 1.79 | 0.98 | 0.50 | ... |

[a] Diameter of the digital circular aperture in arcseconds. The 10″ aperture photometry of source C is given for comparison with the photometry of Carico et al. 1988.

[b] Integrated $K$-magnitude within the aperture.

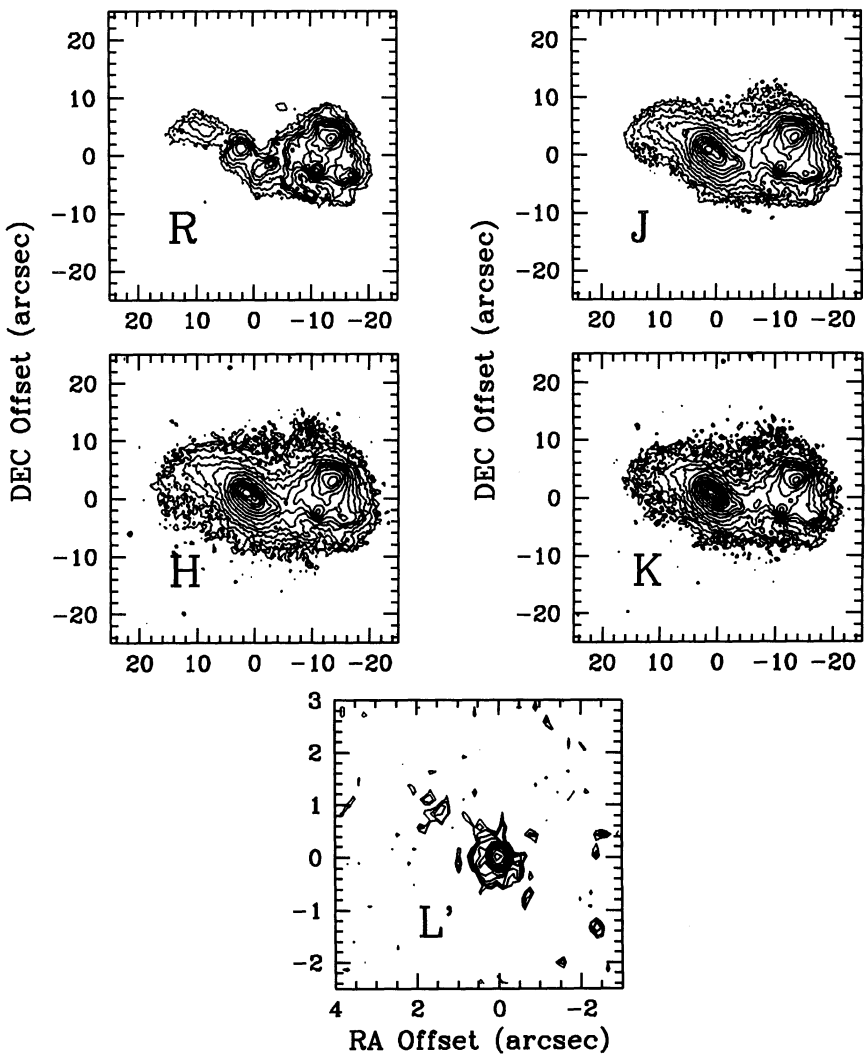


FIG. 1.—Contour plots of VV 114 in the optical ($R$) and the infrared ($JHKL'$). North is up and east is to the left. The origins of the plots are defined by the brightest 2.2 $\mu$m knot (source A) whose position is determined to be $\alpha_{1950} = 01^h05^m19^s.82$, $\delta_{1950} = -17°46'25''.7$.

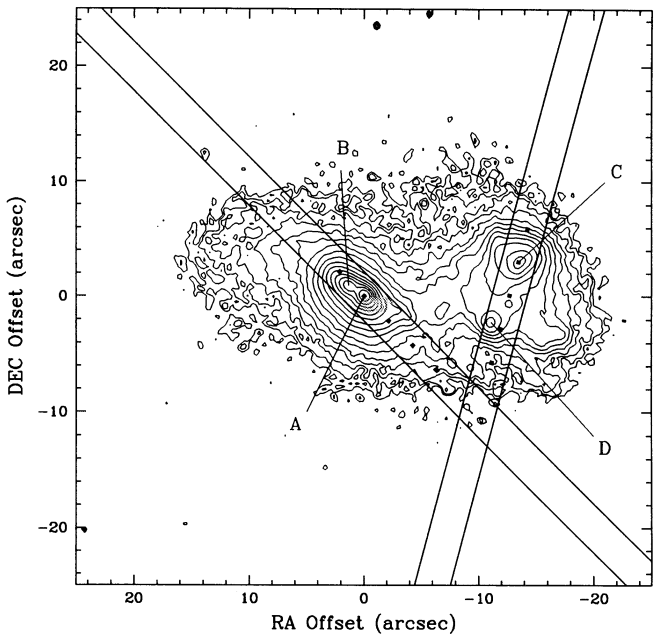


FIG. 2.—*K*-band image of VV 114. The main centers of interest are noted by the letters A, B, C, and D. Parallel lines indicate the orientation of the CGS4 slit. Positions where spectra were extracted are indicated by the squares.

positions are identified in Figure 2 as squares. The extracted spectra are shown in Figure 3, and the line fluxes and equivalent widths of the dominant emission and absorption lines are listed in Table 2. The positions given in Table 2 are relative to the position where the slit was centered. Position "0" corresponds to source A in VV 114E and source C in VV 114W. The other positions are expressed by their relative offset to the central position, a negative offset corresponding to the southwest and the southeast in VV 114E and VV 114W, respectively. We note that the position VV 114W-6 is only a few arcseconds away from source D. Also, one must bear in mind that because the effective aperture of the spectrometer is 3″ × 3″, and the separation between sources A and B is only 1.″6, the spectrum of source A shown in Figure 3*a* is significantly contaminated by the nearby source B.

As seen in Figures 3*a* and 3*b*, the overall slope of the continuum (i.e., the spectral index) varies with position. In general, the continuum of VV 114E is redder than VV 114W, which is consistent with the colors derived from aperture photometry (see Table 1). Note the abrupt variation in the spectral index between source A and the position 3″ NE (close to source B). The spectrophotometry obtained by averaging the spectra of sources A and 3″ NE is ~25% fainter than the corresponding photometry derived by projecting a digital slit with pixels of 3″ × 3″ on the *K* image. This discrepancy is not significant and could be due to a slight pointing error. Indeed, this discrepancy could be explained if the slit was centered 1″ ($\frac{1}{3}$ of a CGS4 pixel) east of the nominal offset for source A (14″ east and 3″ south) with respect to the optical peak (source C).

The CO absorption band longward of 2.3 $\mu$m is detected at most positions. We have estimated the strength of the CO band using the spectroscopic CO index ($CO_{sp}$) as defined by Doyon, Joseph, & Wright (1994). $CO_{sp}$ is defined as the average of the rectified spectrum between 2.31 and 2.4 $\mu$m on a magnitude scale. This index is very much like the photometric CO index (e.g., Frogel et al. 1978), increasing with deeper CO bands. For the purpose of rectifying the spectra, the continuum was determined by fitting a power-law ($F_\lambda \propto \lambda^\alpha$) from featureless sections of the spectrum, defined so as to avoid the spectral range of prominent (or potential) emission and absorption lines. The emission lines avoided are He I 2.06 $\mu$m, Br$\gamma$, 1–0 *S*(0), 1–0 *S*(1) and the 2–1 *S*(1) of $H_2$. The Na I doublet (~2.206) and the Ca II triplet (~2.263) which are seen in absorption in late-type stars (Kleinmann & Hall 1986) were also avoided. Since some spectra show an apparently strong absorption feature near 2.06 $\mu$m which is likely the result of an imperfect correction of a strong $CO_2$ atmospheric feature, this spectral range was excluded for fitting the continuum. The power-law fits are represented by the continuous solid line in Figure 3. Spectroscopic CO indices are given in Table 2 for each position. For comparison, normal giant-dominated galaxies (ellipticals, bulges of spirals) have typical $CO_{sp}$ of 0.2 ± 0.02 (Doyon et al. 1994). In general, a $CO_{sp}$ larger than 0.2 provides some evidence for the presence in the stellar population of red supergiants which have deeper CO bands than giants.

The detection of the CO band in VV 114 shows that a significant fraction of the *K* continuum in this galaxy has a stellar origin. Another important aspect of the CO band is its gradient, i.e., the variation of the CO band strength as a function of position on the galaxy. In general, most galaxies show negligible CO index gradients (Frogel et al. 1978), suggesting a uniform stellar population. This is far from the case in VV 114, where the $CO_{sp}$ varies from 0 to 0.3 mag (see Table 2). The

TABLE 2

LINE FLUXES AND CO BAND STRENGTHS IN VV 114

| Position | 1–0 *S*(1) ($10^{-18}$ W m$^{-2}$) | 1–0 *S*(0) ($10^{-18}$ W m$^{-2}$) | 2–1 *S*(1) ($10^{-18}$ W m$^{-2}$) | *Q*-branch ($10^{-18}$ W m$^{-2}$) | He I λ2.06 ($10^{-18}$ W m$^{-2}$) | Br$\gamma$ ($10^{-18}$ W m$^{-2}$) | $W_{Br\gamma}$ (Å) | $CO_{sp}$ (mag) |
|---|---|---|---|---|---|---|---|---|
| VV 114 East | | | | | | | | |
| −9″ SW | 1.85 ± 0.2 | <0.6 | <0.6 | ... | <0.6 | 1.20 ± 0.2 | 67.6 ± 1 | 0.32 ± 0.11 |
| −6″ SW | 1.55 ± 0.2 | <0.6 | <0.6 | ... | <0.6 | 2.47 ± 0.2 | 72.8 ± 1 | 0.01 ± 0.03 |
| −3″ SW | 1.77 ± 0.3 | <0.9 | <0.9 | ... | <0.9 | 4.34 ± 0.3 | 32.7 ± 1 | 0.03 ± 0.02 |
| 0 (Source A) | 6.92 ± 0.5 | 3.38 ± 0.5 | 2.67 ± 0.5 | ... | 5.48 ± 0.5 | 14.9 ± 0.5 | 27.8 ± 1 | 0.12 ± 0.01 |
| +3″ NE | 4.13 ± 0.3 | 1.93 ± 0.3 | 0.6 ± 0.3 | ... | 2.15 ± 0.3 | 5.22 ± 0.3 | 13.3 ± 1.5 | 0.19 ± 0.02 |
| VV 114 West | | | | | | | | |
| −9″ SE | 0.8 ± 0.3 | <0.9 | <0.9 | <0.9 | <0.9 | 1.73 ± 0.3 | 72 ± 2 | 0.06 ± 0.04 |
| −6″ SE | 2.79 ± 0.3 | 1.09 ± 0.3 | 0.70 ± 0.3 | 3.24 ± 0.3 | 3.18 ± 0.3 | 7.13 ± 0.3 | 74.8 ± 1 | 0.31 ± 0.03 |
| −3″ SE | 3.62 ± 0.3 | 1.33 ± 0.3 | 1.01 ± 0.3 | 7.43 ± 0.3 | 1.37 ± 0.3 | 3.64 ± 0.3 | 25.5 ± 1 | 0.11 ± 0.04 |
| 0 (Source C) | 3.00 ± 0.3 | 1.54 ± 0.3 | 1.00 ± 0.3 | 4.0 ± 0.5 | 2.03 ± 0.3 | 3.33 ± 0.3 | 13.5 ± 0.5 | 0.21 ± 0.02 |
| +3″ NW | 0.57 ± 0.3 | <0.9 | <0.9 | 4.96 ± 0.3 | <0.9 | 1.38 ± 0.3 | 15.7 ± 0.5 | 0.05 ± 0.04 |

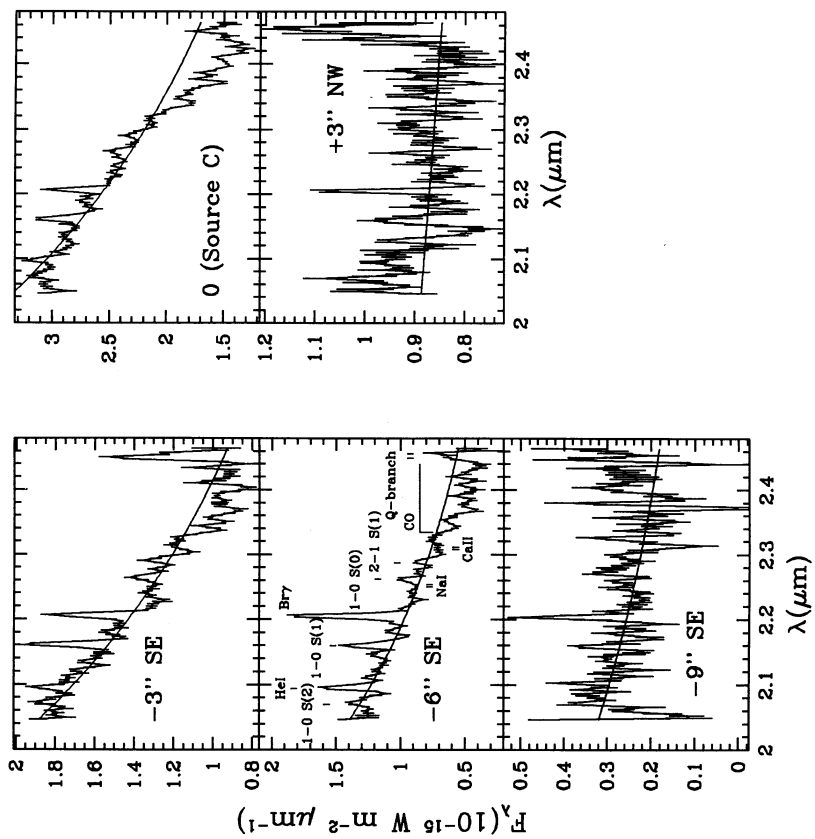


FIG. 3b

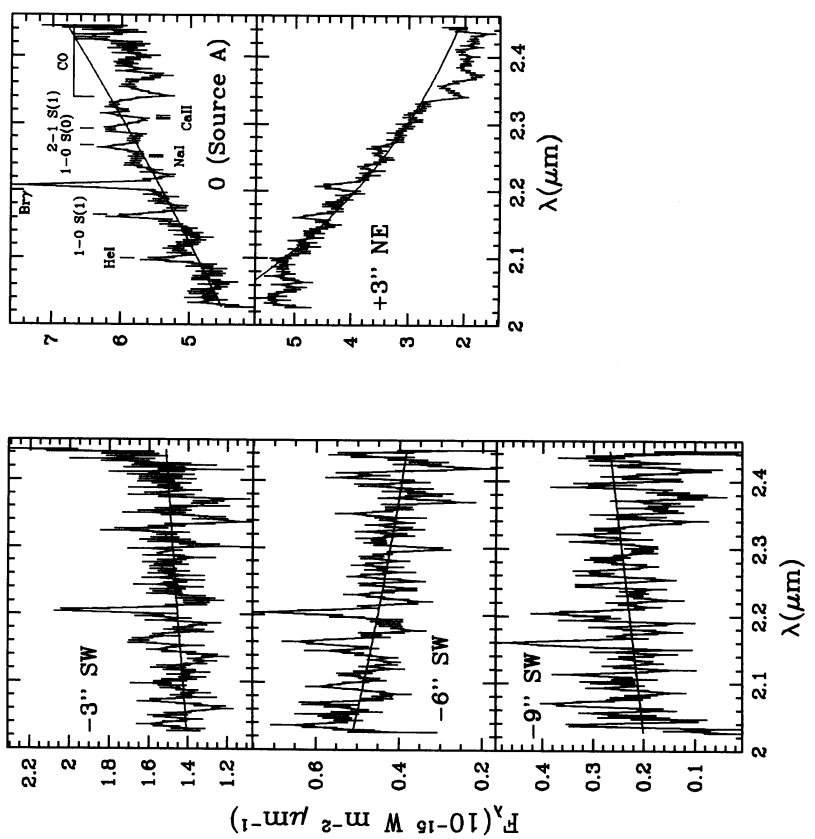


FIG. 3a

FIG. 3.—(*a*) *K*-band spectra extracted from the eastern part of VV 114. Each point is plotted with an error bar of $\pm 1\,\sigma$. The solid lines are the best power-law fits of the continuum (see text). The expected position of several transitions is indicated at the top of the figure. (*b*) Same as (*a*) but for the western (optical) part of the galaxy.

highest indices indicate the presence of red supergiants in VV 114. However, the strongest CO bands (VV 114E-9, VV 114E-6) are not detected on the strongest IR sources. Indeed, sources A and B have a relatively modest $CO_{sp}$ of $0.12 \pm 0.01$ and $0.19 \pm 0.02$, respectively. We shall see later that such a small $CO_{sp}$ is not necessarily incompatible with the presence of numerous red supergiants, since the CO band can be heavily diluted by hot dust emission, early-type stars, and nebular emission, which have no CO absorption. The stellar origin of the *K* continuum of the VV 114 spectra is further confirmed by the detection of the Ca II triplet at some positions, including source A, VV 114W-3SE, and VV 114W-6SE.

The strongest emission lines detected are Br$\gamma$ (observed at $\sim$2.21 $\mu$m), He I 2.06 $\mu$m (at 2.10 $\mu$m), and the 1–0 *S*(1) line of $H_2$ (at $\sim$2.17 $\mu$m). Although much fainter, other transitions of $H_2$, including the 1–0 *S*(0), 2–1 *S*(1), and the *Q*-branch, are also detected in some positions (see Table 2). The strongest emission lines are found in source A. The fact that both Br$\gamma$ and He I 2.06 $\mu$m are spectrally unresolved suggests that the gas is photoionized by young OB stars associated with an episode of vigorous star formation activity, and not by an AGN-like object. The detection of recombination lines outside the main IR sources indicates that the star formation is widespread throughout the galaxy.

Despite the modest resolution of our spectra, the detection of several emission lines allows us to measure velocity gradients across VV 114 with a reasonable accuracy. Average recessional velocities were determined by fitting a Gaussian profile to every emission line detected in a given spectrum, that is, those listed in Table 2 with a clear detection. The error assigned to the average velocity inferred for a given spectrum was simply taken as the standard error of the data set. Here we made the assumption that both the molecular gas ($H_2$ emission) and the ionized gas (Br$\gamma$ and He I 2.06 $\mu$m) share the same kinematics.

The velocity gradients observed in VV 114 are shown in Figure 4. The velocity gradient of VV 114E has the typical S-shape characteristic of a rotation curve, with a systemic velocity of $5953 \pm 75$ km s$^{-1}$ and a velocity gradient of $\sim$158 km s$^{-1}$ per kpc. An unusual aspect of this rotation curve is the fact that its center of symmetry is not coincident with either of the two strong sources (A and B) found in the vicinity; i.e., it is located somewhere 3″ southwest of source A. We stress that this result cannot be an instrumental artifact. For instance, the tilt of the spectrum mentioned in § 2.2.2 is far too small ($\sim$0.″4) to explain the observed gradient. The most likely explanation of this offset is probably that the CGS4 slit was not perfectly centered on source A—which would explain the apparent discrepancy between the *K*-band photometry and spectrophotometry, as mentioned earlier—and misaligned with respect to the major axis of the underlying galaxy. This alignment is very critical if the system is seen nearly edge-on. In this context, if we assume that the dynamical center is centered on either sources A or B, then the offset observed between these positions and the center of symmetry of the rotation curve probably implies that VV 114E is seen nearly edge-on. From this rotation curve we infer a mass ($rv^2/G$) enclosed within the central 1.1 kpc of $9 \times 10^9$ $M_\odot$, which is similar to the mass of our Galaxy within the same radius. This is also consistent with the total $H_2$ mass of $5.1 \times 10^{10}$ $M_\odot$ as derived from the CO emission measured in a $6 \times 3$ kpc region centered on VV 114E (Yun et al. 1994).

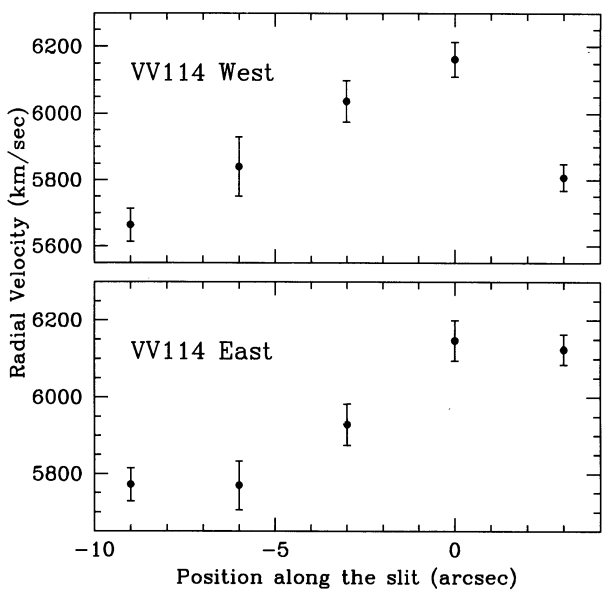


FIG. 4.—Velocity gradient observed along the slit. The positive direction is to the southeast for VV 114 West and to the southwest for VV 114 East.

The velocity gradient of VV 114W does not show a well-defined rotation curve such as observed for VV 114E, but it is similar in magnitude (145 km s$^{-1}$ per kpc), implying that both regions have approximately the same dynamical mass. The systemic velocity of VV 114W is not significantly different from that of VV 114E, confirming that both regions are seen at the same distance and interacting in the plane of the sky. Knop et al. (1994) reached the same conclusion based on their optical spectroscopy.

## 4. DISCUSSION

### 4.1. *Starburst or AGN?*

Our near-IR images and spectroscopy put strong constraints on the origin of the FIR luminosity emitted by VV 114. First, it is clear that the center of activity is not, as previously thought, concentrated on the optical part of the galaxy. It is more natural to associate the center of activity with the brightest IR sources, namely A and B. As argued by Knop et al. (1994), the spatial coincidence between these two near-infrared sources with a similar radio structure (Condon et al. 1991), combined with the fact that the two sources have a similar flux ratio, strongly suggests that VV 114E is a merger. This hypothesis is supported by noncircular gas motions detected in CO (Yun et al. 1994) in VV 114E. The near-infrared morphology of the VV 114 system leaves little doubt that the merger in VV 114E is interacting with a third galaxy whose dynamical center is probably located near source C.

The fact that the main sources of this galaxy show extended emission at 2.2 $\mu$m is very suggestive that the near-IR continuum has a stellar origin and is not produced by an AGN-like engine that would manifest itself as a point source. The only way for an AGN to be the source of the FIR luminosity and show extended emission at 2.2 $\mu$m is for the AGN to be deeply buried under a dense veil of dust, and totally opaque to near-IR radiation. The fact that source A is undetected in the optical and unresolved at *L* could argue in favor of this hypothesis, but the radio data weaken this possibility, because source A is clearly extended at 20 cm (Condon et al. 1991).

Further evidence for star formation activity is provided by the *JHK* colors of the object. A two-color diagram ($J-H$ vs.

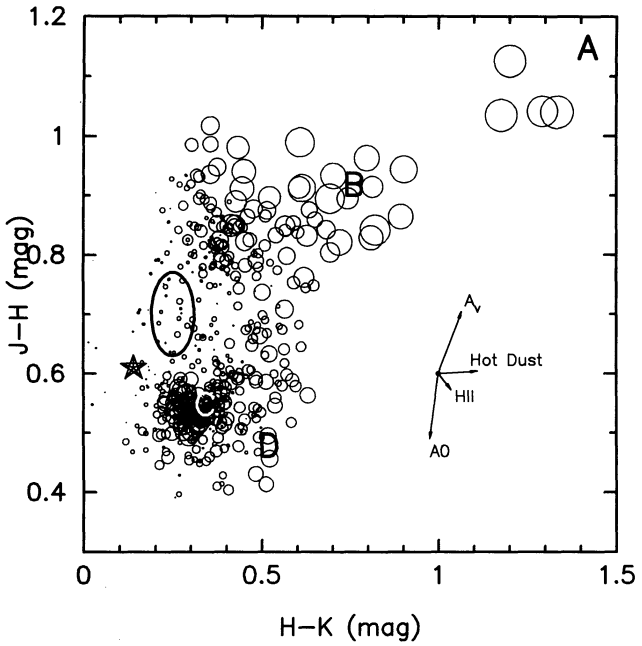


FIG. 5.—Two-color diagram of VV 114. Each symbol represents the color of an individual pixel determined after combining the fluxes in 3 × 3 pixels (0.″75 × 0.″75) from the original images. Only pixels brighter than $m_k = 18.5$ are shown. The size of the symbols is proportional to the $K$ brightness of the pixel on a magnitude scale (the brighter the pixel, the larger the symbol). Loci of colors for normal galaxies are indicated by the ellipse. The color of a K5I is indicated by the "star." The arrows show the effect on the $JHK$ colors due to one magnitude of visual extinction ("$A_V$"), 10% contamination of the $K$ continuum by hot dust, nebular emission ("H II"), and blue stars ("A0"). The colors of the sources A, B, C, and D inferred from a 1″ aperture are indicated by large capital letters. Symbol "C" is shown white on black.

$H-K$) of VV 114 is presented in Figure 5. The diagram shows colors of individual pixels, obtained after binning the original image by a factor of three (0.″75 × 0.″75), with the size of the symbols proportional to the $K$ brightness of the pixel (the brighter the pixel, the larger the symbol). For comparison, the range of colors observed in nuclei of late-type spirals ($H-K = 0.25 \pm 0.06$ and $J-H = 0.70 \pm 0.07$; Frogel 1985) are represented by the ellipse. The effects on the $JHK$ colors of extinction and 2.2 $\mu$m continuum contamination from blue stars (A0V), nebular (free-free + bound-free), and hot dust emission, are indicated by the arrows. The colors of a red supergiant star (K5I) are also indicated by the "star" for comparison.

The first point to note is that the scatter in the two-color diagram is much greater than that observed in normal galaxies, showing that other processes at work in VV 114 alter the normal colors of the background stellar population. It is clear from Figure 5 that the VV 114E regions (sources A and B) have colors that differ markedly from those observed in VV 114W (sources C and D). The VV 114W regions have colors like those of sources C and D, following closely the nebular emission vector with a possible contribution from blue stars. The position of sources C and D in the color-color diagram suggest that nebular emission contributes between 30% and 70% of the 2.2 $\mu$m continua of those regions. Extinction does not seem to significantly affect the colors of these sources. The two-color diagram clearly demonstrates that extinction alone cannot explain the very red colors of sources A and B and that another component, such as hot dust, is needed.

The presence of numerous OB stars in VV 114E is confirmed by the detection of the recombination lines Br$\gamma$ and He I 2.06 $\mu$m. As shown in Doyon et al. (1992), the He I 2.06 $\mu$m/Br$\gamma$ can be used to characterize the average spectral type of a young stellar population. They show that this ratio is a steep function of the effective temperature, a property that can be used to put some constraints on the upper mass limit of the initial mass function (IMF). Although Shields (1993) showed that the relationship between spectral type and He I 2.06 $\mu$m/Br$\gamma$ ratio is ambiguous, this ratio still provides a useful diagnostic for characterizing approximately the average spectral type of a young stellar population. Both sources A and B have a similar He I 2.06 $\mu$m/Br$\gamma$ of $\sim$0.4 which corresponds to a spectral type earlier than O8V. The observed Br$\gamma$ luminosity (corrected for an extinction $A_K = 0.4$ mag) in the central 1 kpc of source A is $4.1 \times 10^6\ L_\odot$ or a total ionization rate of $1.2 \times 10^{54}$ photons $s^{-1}$, which is the equivalent output of $7.3 \times 10^4$ O8V stars. For comparison, the ionization rate in the central 600 pc of the nearby starburst M82 is $1.1 \times 10^{54}$ photons $s^{-1}$ (Puxley et al. 1989). Thus, the starburst magnitude in source A is similar to that in M82.

The Br$\gamma$ luminosity profile in VV 114E is very well approximated with an exponential distribution with a scale length of 1.4 kpc. If we extrapolate this exponential distribution to the whole region of VV 114E, we can infer a total Br$\gamma$ luminosity (uncorrected for extinction) of $2.3 \times 10^7\ L_\odot$, equivalent to a cluster of $4 \times 10^5$ O8V stars with a corresponding bolometric luminosity of $2.5 \times 10^{11}\ L_\odot$, which is more than half the total *IRAS* luminosity. This shows that a large fraction of the energy output of the whole VV 114 system is contributed by VV 114E.

In summary, both the infrared imaging and spectroscopy suggest that a starburst, as opposed to an AGN, is the most likely luminosity source of VV 114. A large fraction of the bolometric luminosity of the whole VV 114 system is emitted from VV 114E.

### 4.2. *The Spectral Energy Distribution of VV 114E*

The color-color diagram presented in the previous section shows that the intrinsic spectral energy distribution (SED) of VV 114 is affected by three components, namely blue stars/nebular emission, hot dust, and extinction. In this section, we investigate further how we can put more constraints on not only the relative contribution from these components, but also on the nature of the underlying spectrum, whether it is a giant or supergiant-type SED. We shall attempt to fit the SEDs of sources A and B.

It is easy to estimate the contribution of blue stars at $K$ from the number of O8V stars derived earlier. Assuming a Salpeter IMF (1955) and that ionizing stars have masses greater than $\sim 20\ M_\odot$, we estimate that there are $5 \times 10^6$ main-sequence stars earlier than A0 ($M \sim 3\ M_\odot$) in the central kpc of source A. Assuming that these stars have an average spectral type B5V with an absolute $K$-magnitude $M_K = -0.7$, as derived from the data of Johnson (1966) and Landolt-Börnstein (1982), we estimate that less than 1% of the $K$ continuum of source A is contributed by these young blue stars. We shall therefore neglect the contribution from blue stars in the following analysis.

The $JHK$ color-color diagram is somewhat restrictive for fitting the SED. We have other information that we can use, including the $R$ and $L'$ photometry and the spectroscopic CO index $CO_{sp}$. Like $JHK$, the $R$ band is sensitive to the presence of nebular emission, whereas the $L'$ band is sensitive to hot

dust. The $CO_{sp}$ is not only dependent on spectral type and luminosity; it depends critically on both the magnitude of the hot dust emission and the contribution from nebular emission at $K$. Both hot dust and nebular emission have the effect of diluting the CO band.

We have used the following simple three-component model to fit the SEDs of sources A and B. First we assume an underlying "cold" continuum for the galaxy which can be either the SED of a normal galaxy or a supergiant with spectral type K5I. This spectral type is chosen because its $CO_{sp}$ is typical of galaxies with strong CO bands (e.g., NGC 3256; Doyon et al. 1994). The intrinsic $RJHKL$ colors and $CO_{sp}$[3] of the K5I star were taken from Elias, Frogel, & Humphreys (1985). The SED assumed for a normal galaxy is: $R-K = 2.42$, $J-K = 0.95$, $H-K = 0.25$, $CO_{sp} = 0.20$ (Frogel 1985), and $K-L = 0.30$ (Joseph et al. 1984). The nebular spectrum was taken from Ferland (1980), with $T_e = 10{,}000$ K. Hot dust ($F_{HD}$) and H II ($F_{H\,II}$) components are then added to the underlying spectrum, and the resulting SED is modified with an extinction at 2.2 $\mu$m ($A_K$). Both $F_{HD}$ and $F_{H\,II}$ represent the fraction of the 2.2 $\mu$m continuum contributed by hot dust and nebular emission, respectively. The extinction law adopted is that of Draine (1989), that is, $A_\lambda \propto \lambda^{-1.75}$. Here we assume a simple "slab" (foreground) model for the dust distribution; that is, we suppose that the emitting sources are not mixed with the dust. This could well be an oversimplification of the problem, but our goal here is not to obtain an accurate estimate of the extinction, but rather to gauge the relative importance of several processes affecting the SED of VV 114E. We note that if the dust is uniformly mixed with the stars, then the extinction derived under the assumption that it is foreground will be systematically underestimated. For the hot dust component, a simple blackbody with emissivity varying linearly with frequency was assumed. We have experimented with dust temperatures of 500, 800, and 1000 K. The synthetic SED is then compared with the observations (2″ aperture photometry and $CO_{sp}$). Since the model uses $L$ (3.4 $\mu$m) band photometry, our $L'$ (3.8 $\mu$m) fluxes were converted to $L$ by interpolation from the observed SED. The reduced $\chi^2$ was used to quantify the goodness of the SED fit. The results are summarized in Table 3. For a given cold component (spectral type) and dust temperature $T_{Dust}$, we give the best combination of $F_{H\,II}$, $F_{Dust}$, and $A_K$ that fit the observed SED.

It is clear from Table 3 that the extinction toward source A is weakly dependent on the spectral type of the underlying continuum and the dust temperature assumed. All models yield an extinction $A_K$ between 0.4 and 0.6 mag with a very large fraction ($\sim$50%) of nonstellar continuum, mostly in the form of hot dust emission. The best SED fits are obtained for an intermediate dust temperature of $\sim$800 K, irrespective of the underlying cold component adopted. A supergiant star as underlying continuum provides the best fit, but this result is not very significant, as judged from the $\chi^2$. This analysis yields that $\sim$50% of the $K$ continuum in source A is due to hot dust with a marginal contribution ($\sim$5%) from nebular emission and that a significant fraction of the remaining continuum may be the result of young late-type red supergiants. The foreground extinction at 2.2 $\mu$m toward source A is $0.5 \pm 0.1$ mag.

The analysis yields an extinction $A_K = 0.3$ mag toward source B which is remarkably similar to that derived for source A. The contribution from nonstellar continuum is much smaller in source B, between 10% and 30%, as opposed to $\sim$60% for source A. The models for source B are insensitive to either the dust temperature or the cold component adopted. There is no evidence for a significant contribution of late-type supergiants in source B. This analysis shows that the relative reddening of sources A and B, as observed in the near-IR, is not the effect of extinction, but due mainly to different contributions of nonstellar emission (mostly hot dust) at 2.2 $\mu$m. It is interesting to note that if we exclude the contribution from nonstellar continuum, source B should be intrinsically as bright (and even brighter, depending on the relative extinction of both sources), as source A.

TABLE 3

SPECTRAL ENERGY DISTRIBUTION FITS OF SOURCES A AND B

| Spectral Type[a] | $F_{H\,II}$ | $T_{dust}$ (K) | $F_{Dust}$ | $A_K$ (mag) | $\chi^2_{red}$ |
|---|---|---|---|---|---|
| | | Source A | | | |
| "Normal"..... | 0.52 | 500 | 0.16 | 0.54 | 11.5 |
| | 0.04 | 800 | 0.44 | 0.42 | 2.4 |
| | 0.14 | 1000 | 0.44 | 0.44 | 6.8 |
| K5I ..... | 0.70 | 500 | 0.14 | 0.56 | 13.4 |
| | 0.06 | 800 | 0.54 | 0.40 | 1.5 |
| | 0.14 | 1000 | 0.54 | 0.42 | 6.3 |
| | | Source B | | | |
| "Normal"..... | 0.06 | 500 | 0.04 | 0.35 | 0.9 |
| | 0.02 | 800 | 0.08 | 0.34 | 1.0 |
| | 0.02 | 1000 | 0.08 | 0.34 | 1.3 |
| K5I ..... | 0.30 | 500 | 0.06 | 0.38 | 2.8 |
| | 0.08 | 800 | 0.26 | 0.32 | 0.4 |
| | 0.00 | 1000 | 0.34 | 0.29 | 1.0 |

[a] "Normal" refers to the SED of a normal galaxy.

Perhaps the most interesting result of this analysis is that both sources A and B suffer from almost the same extinction. There is no reason why this should be the case for two regions of VV 114E separated by 600 pc with different SEDs. One likely explanation is that the extinction is mostly *foreground*, perhaps due to a dust lane or a bar. It would be worthwhile to investigate this question further by observing several recombination lines of hydrogen from 1 to 5 $\mu$m, since those could be used for determining the relative contributions of internal and foreground extinction, as shown by Puxley (1991) (see also Puxley & Brand 1994).

### 4.3. *Excitation and Origin of the* $H_2$ *Emission*

The detection of $H_2$ emission in VV 114 is not very surprising, since this is a typical spectral feature observed in starburst galaxies. Most previous studies of $H_2$ emission in starbursts have concentrated in general on the *nuclear* $H_2$ emission. The fact that we have detected the $H_2$ outside the main centers of activity of VV 114 offers us a unique opportunity to study the $H_2$ emission in the circumnuclear regions of starbursts. In the following sections, we discuss the origin and excitation mechanism of the $H_2$ emission observed in VV 114.

The $H_2$ gas can be excited either by shocks or UV fluorescence. Shock-excited $H_2$ emission is conspicuous in star-forming regions, such as the Orion nebula and in supernova remnants. On a larger scale, the $H_2$ emission can be excited by interaction-driven shocks; the most celebrated example is the galaxy NGC 6240 (Herbst et al. 1990; van der Werf et al. 1993).

[3] $CO_{sp}$ was derived from the photometric CO index $CO_{ph}$ using the transformation given in Doyon et al. (1994).

Fluorescently excited $H_2$ emission is expected when there are enough ultraviolet (UV) photons to excite the surrounding molecular gas. Since star-forming regions, supernova remnants, and the production of relatively strong UV fluxes are all natural by-products of starburst activity, it is not surprising qualitatively speaking, to find $H_2$ emission in starbursts. What is more challenging is to determine which of these mechanisms dominates, if one does at all.

One way to discriminate between shock-excited and fluorescently excited $H_2$ emission is to measure the 2–1 $S(1)$/1–0 $S(1)$ and 1–0 $S(0)$/1–0 $S(1)$ line ratios, which are expected to be 0.1 and 0.2 in the shock case (Hollenbach & Shull 1977), but as high as 0.5 and 0.6 in the fluorescent case (Black & van Dishoeck 1987). The latter ratios are valid for relatively low densities ($< 10^4$ cm$^{-3}$), beyond which the high vibrational levels of $H_2$ become collisionally deexcited or thermalized, resulting in a spectrum that mimics shock excitation (Sternberg & Dalgarno 1989). Despite this ambiguity, these line ratios still represent a very useful diagnostic of the excitation mechanism of the $H_2$ gas.

As shown in Figure 3, these diagnostic lines are clearly detected on VV 114E (source A), VV 114W (source C), VV 114W-3, and VV 114W-6 (close to source D). Using the line fluxes listed in Table 2, we infer 1–0 $S(0)$/1–0 $S(1)$ line ratios varying between 0.4 and 0.5 and 2–1 $S(1)$/1–0 $S(1)$ line ratios ranging from 0.25 and 0.49. The highest line ratios are observed on source A. Clearly, these line ratios are more consistent with UV fluorescence than shock excitation. Although, given the relatively low resolution of our spectra, we cannot exclude the possibility that we have systematically overestimated the strengths of the 2–1 $S(1)$ and 1–0 $S(1)$ by misplacing the nearby continuum, this uncertainty should not exceed $\sim$50% of the line fluxes quoted in Table 2. Thus, despite these uncertainties, it is safe to conclude that the 2–1 $S(1)$/1–0 $S(1)$ and 1–0 $S(0)$/1–0 $S(1)$ line ratios observed in most regions of VV 114 are intermediate between the values expected for thermal and fluorescent excitation. The average 2–1 $S(1)$/1–0 $S(1)$ and 1–0 $S(0)$/1–0 $S(1)$ line ratios observed in VV 114, 0.31 and 0.44, respectively, imply that 50%–60% of the 1–0 $S(1)$ flux is contributed by the fluorescent component. However, because only 1% of the total emission at all wavelengths from $H_2$ excited by low-density fluorescence is emitted in the 1–0 $S(1)$, as opposed to 10% for shock excitation (Black & van Dishoeck 1987), UV fluorescence should contribute more than 90% of the total $H_2$ emission in VV 114.

The 1–0 $S(1)$/Br$\gamma$ ratio also provides some constraints on the excitation mechanism. In Figure 6, we have plotted the 1–0 $S(1)$ and Br$\gamma$ fluxes for all positions in VV 114. There is a significant positive correlation between the emission lines, showing that there is a close association between the excitation of the $H_2$ gas and star formation activity. A similar correlation exists for galaxies in general (Puxley, Hawarden, & Mountain 1990). Such a correlation could be explained by assuming that the $H_2$ emission is fluorescently excited; the more UV photons are available to excite the molecular gas, the more $H_2$ emission is produced. This is the interpretation favored by Puxley et al. (1990). Although this correlation is consistent with the fluorescence scenario, it does not prove by itself that the $H_2$ emission is fluorescently excited; it just strengthens the case for it. Indeed, it is possible that the $H_2$ emission could be shock-excited by young supernova remnants, in which case, if the timescale of the starburst event is similar to or longer than the lifetime of O stars, then one should expect a positive correlation between the $H_2$ and Br$\gamma$ emissions.

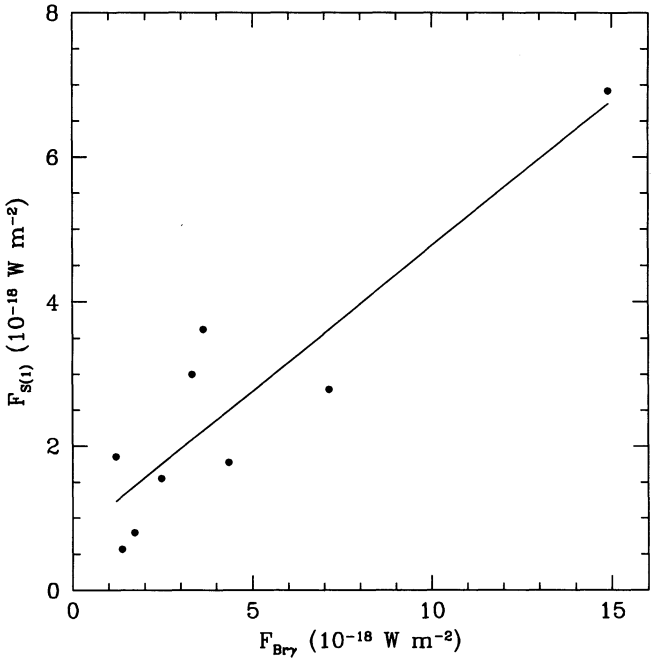


FIG. 6.—1–0 $S(1)$ vs. Br$\gamma$ fluxes for all positions of VV 114

The evidence for UV fluorescence presented here is only marginal, and higher spectral resolution observations will be needed to more accurately determine the fraction of $H_2$ emission excited by fluorescence in VV 114. Observations of the [Fe II] line at 1.644 $\mu$m, a very strong feature in supernova remnants, would also be desirable, since it would help to determine the contribution from shock-excited $H_2$ emission associated with these remnants.

## 5. SUMMARY AND CONCLUSIONS

We have presented optical/near-IR images and $K$-band spectra of the bright *IRAS* galaxy VV 114. The main results of this study are as follows.

1. The morphology of VV 114 in the infrared differs markedly from the optical. The infrared images have unveiled a region containing two strong infrared sources located $\sim$15″ east of the main optical peak. This region is barely detected in the optical.

2. The $JHK$ colors of the optical part of VV 114 suggest that the 2.2 $\mu$m continuum has a large contribution (up to 70%) from blue stars and nebular emission associated with H II regions. The morphology of this region is likely due to the presence of numerous H II regions in the vicinity of a single galaxy.

3. $K$-band spectra obtained at several positions in VV 114 show strong emission lines of He I 2.06 $\mu$m, Br$\gamma$, several transitions of $H_2$ emission, and deep 2.3 $\mu$m CO band. The bulk of the $H_2$ emission is probably excited by UV fluorescence.

4. A velocity gradient typical of a rotation curve was observed near the two brightest IR sources of VV 114. The center of symmetry of the rotation curve does not appear to be coincident with any of this sources. This offset could be explained if the underlying galaxy is seen nearly edge-on. Analysis of the SEDs of these two sources reveals that they are both affected by an extinction $A_K$ of $\sim$0.4 mag. As much as 50% of the $K$ continuum of the brightest source is contributed

by hot dust emission. The remaining continuum is produced by young late-type supergiants.

It is a pleasure to thank all the CFHT and UKIRT staff, and particularly the telescope operators John Hamilton, Ken Barton, Norman Purves, and Joel Aycock and the support scientists Doug Simons and Tom Geballe for their invaluable assistance in obtaining these observations. We are grateful to Richard Baron, who took the $L'$ images on IRTF. We thank the anonymous referee for very useful comments. R. D., D. N., and N. R. acknowledge financial support from the Natural Science and Engineering Research Council of Canada.

## REFERENCES

Allen, D. A., Norris, R. P., Meadows, V. S., & Roche, P. F. 1991, MNRAS, 248, 528
Becklin, E. E., & Wynn-Williams, C. G. 1987, in Star Formation in Galaxies, ed. C. J. Lonsdale-Persson (NASA Conf. Publ. No. 2466) 643
Black, J. H., & van Dishoeck, E. F. 1987, ApJ, 322, 412
Carico, D. P., Sanders, D. B., Soifer, B. T., Elias, J. H., Matthews, K., & Neugebauer, G. 1988, AJ, 95, 2
Casali, M., & Hawarden, T. 1992, JCMT-UKIRT Newsletter, No. 4, 33
Condon, J. J., Huang, Z. P., Yin, Q. F., & Thuan, T. X. 1991, ApJ, 378, 65
Doyon, R., Joseph, R. D., & Wright, G. S. 1994, ApJ, 421, 101
Doyon, R., Puxley, P. J., & Joseph, R. D. 1992, ApJ, 397, 117
Draine, B. T. 1989, in Proc. 22d ESLAB Symposium, Infrared Spectroscopy in Astronomy, ed. B. H. Kaldeich (Paris: ESA Pub. Div.), 93
Elias, J. H., Frogel, J. A., & Humphreys, R. M. 1985, ApJS, 57, 91
Ferland, G. J. 1980, PASP, 92, 596
Frogel, J. A. 1985, ApJ, 298, 528
Frogel, J. A., Persson, S. E., Aaronson, M., & Matthews, K. 1978, ApJ, 220, 75
Goldader, J. D., Joseph, R. D., Doyon, R., & Sanders, D. B. 1995, ApJ, 444, 97
Herbst, T. M., Graham, G. R., Beckwith, S., Tsutsui, K., Soifer, B. T., & Matthews, K. 1990, AJ, 99, 1773
Hollenbach, D., & Shull, J. M. 1977, ApJ, 216, 419
Johnson, H. L. 1966, ARA&A, 4, 193
Joseph, R. D., Meikle, W. P. S., Robertson, N. A., & Wright, G. S. 1984, MNRAS, 209, 111
Joseph, R. D., & Wright, G. S. 1985, MNRAS, 311, 132
Joseph, R. D., Wright, G. S., & Wade, R. 1984, Nature, 311, 132
Kleinmann, S. G., & Hall, D. N. B. 1986, ApJS, 62, 501
Knop, R. A., Soifer, B. T., Graham, J. R., Matthews, K., Sanders, D. B., & Scoville, N. Z. 1994, AJ, 107, 920
Landolt-Börstein, 1982, Astronomy & Astrophysics, 2B, Star & Star Clusters, ed. K. Schiaffers & H. H. Voigt (Berlin: Springer)
Mountain, C. M., Robertson, D. J., Lee, T. J., & Wade, R. 1990, Proc. SPIE, 1235, 25
Nadeau, D., Murphy, D., Doyon, R., & Rowlands, N. 1994, PASP, 106, 909
Norman, C., & Scoville, N. Z. 1988, ApJ, 332, 124
Puxley, P. J. 1991, MNRAS, 249, 11
Puxley, P. J., & Brand, P. W. J. L. 1994, MNRAS, 266, 431
Puxley, P. J., Brand, P. W. J. L., Moore, T. J. T., Mountain, C. M., Nakai, N., & Yamashita, T. 1989, ApJ, 345, 163
Puxley, P. J., Hawarden, T. G., & Mountain, C. M. 1990, ApJ, 364, 77
Rieke, G. H., Lebofsky, M. J., Thompson, R. I., Low, F. J., & Tokanaga, A. T. 1980, ApJ, 238, 24
Salpeter, E. E. 1955, ApJ, 121, 161
Sanders, D. B., Scoville, N. Z., & Soifer, B. T. 1991, ApJ, 370, 158
Sanders, D. B., Soifer, B. T., Elias, J. H., Madore, B. F., Matthews, K., Neugebauer, G., & Scoville, N. Z. 1988, ApJ, 325, 74
Scoville, N. Z., & Norman, C. 1988, ApJ, 332, 163
Scoville, N. Z., Sanders, D. B., Sargent, A. I., Soifer, B. T., & Tinney, C. G. 1989, ApJ, 345, L25
Shields, J. C. 1993, ApJ, 402, 425
Soifer, B. T., Boehmer, L., Neugebauer, G., & Sanders, D. B. 1989, AJ, 98, 766
Soifer, B. T., Sanders, D. B., Madore, B. F., Neugebauer, G., Danielson, G. E., Elias, J. H., Lonsdale, C. J., & Rice, W. L. 1987, ApJ, 320, 257
Sternberg, A., & Dalgarno, A. 1989, ApJ, 338, 197
Telesco, C. M., Decher, R., & Gatley, I. 1985, ApJ, 299, 896
Thompson, R. I., Lebofsky, M. J., & Rieke, G. H. 1978, ApJ, 222, L49
van der Werf, P. P., Genzel, R., Krabbe, A., Blietz, M., Lutz, D., & Drapatz, S. 1993, ApJ, 405, 522
Yun, M. S., Scoville, N. Z., & Knop, R. A. 1994, ApJ, 430, L109